Biochimica et Biophysica Acta 1838 (2014) 994–1002

Contents lists available at ScienceDirect

Biochimica et Biophysica Acta

journal homepage: www.elsevier.com/locate/bbamem

Molecular dynamics simulations of lipid membranes with lateral force: Rupture and dynamic properties

Jun Yu Xie [a,c], Guang Hong Ding [a,b,*], Mikko Karttunen [d,**]

[a] Department of Mechanics Engineering and Science, Fudan University, 220 Handan Rd, Shanghai 200433, China
[b] Shanghai Research Center of Acupuncture and Meridians, 199 Guoshoujing Rd, Shanghai 201203, China
[c] Department of Applied Mathematics, The University of Western Ontario, 1151 Richmond St. North, London, Ontario N6A 3K7, Canada
[d] Department of Chemistry, University of Waterloo, 200 University Avenue West, Waterloo, Ontario N2L 3G1, Canada

ARTICLE INFO

Article history:
Received 12 July 2013
Received in revised form 15 December 2013
Accepted 18 December 2013
Available online 27 December 2013

Keywords:
Lipid membrane
Rupture
Lateral tension
Molecular dynamics simulation

ABSTRACT

Membranes' response to lateral tension, and eventual rupture, remains poorly understood. In this study, pure dipalmitoylphosphatidylcholine (DPPC) lipid bilayers, under tension/pressure, were studied using molecular dynamics (MD) simulations. The irreversible membrane breakdown is demonstrated to depend on the amplitude of lateral tension, loading rate, and the size of the bilayer. In all of our simulations, −200 bar lateral pressure was found to be enough to rupture lipid membrane regardless of the loading rate or the membrane size. Loading rate and membrane size had a significant impact on rupture. A variety of dynamic properties of lipid molecules, probability distribution of area per lipid particularly, have been determined, and found to be fundamental for describing membrane behavior in detail, thus providing the quantitative description for the requirement of membrane rupture.

1. Introduction

Membranes are essential to all living organisms. Mechanical forces act on organisms in a variety of ways. Cells have different mechanisms to respond to mechanical stimuli and convert mechanical signals into electrical or chemical signals, which plays a mechanotransduction role in a number of physiological activities such as cell growth, signal transduction, and transport [1,2]. Lateral membrane tension, caused by mechanical forces, may change the state (open/closed) of membrane channels [3]. Mechanical forces have also an important effect on membrane permeability [4,5]. Both lateral diffusion of lipids [6,7] and the formation of lipid rafts [8] rely, to some extent, on membrane tension. Knowing how lipid membranes respond to changes in lateral tension is crucial to understanding cellular functions. Rupture is an extreme response and may occur due to influence of tension or weakening of a membrane due to detergent as in bacterial disinfectants. Generally, rupture occurs when a membrane reaches its critical lateral tension [9].

The effect of mechanical stress on membranes has been studied extensively by experiments, see e.g. Ref. [10]. For example, the effect of force on sheared endothelial cells [6,7,11] as well as hair cells [12,13] has been studied. Membrane rupture is generally considered to occur at tensions from 1 to 25 mN/m [14]. When fluid membrane vesicles were subjected to a steady ramp of micropipette suction, it was found that the rupture strongly depended on the loading rate [14–16]: At high loading rates (up to 10 mN/m/s), the critical tension was 3–5 times larger than that at low loading rates (1–2 mN/m/s). Lipid composition has been considered to determine rupture strength [4]. Although such experimental techniques have shed considerable light on the properties of membranes, the presence of disorder in these systems greatly limits the nature of the structural data which can be obtained experimentally. The process of rupture is rather fast and involves subtle changes at the molecular level. It is difficult to study the molecular level mechanisms by experimental techniques.

Computational methods offer an alternative approach and MD simulations have been used to study water pore formation and membrane rupture. For example, in previous MD simulation of a pure DPPC bilayer [9], application of a large mechanical pressure of −200 bar led to pore formation (a water channel) and irreversible rupture. Membrane rupture has also been observed in simulations of different mixed bilayers of phosphatidylethanolamine and $C_{12}E_6$, which tried to determine the rupture properties of mixed bilayers of lipid and nonionic surfactant, and explain why dividing cells were more at risk than static cells [17].

Further MD simulations of pure DPPC bilayers showed that water pores, i.e., water channels, could be stabilized under low tension, but became unstable and caused membrane rupture when tension reached about 38 mN/m [18]. Self-organization of a stable pore structure (a sufficient number of water molecules in the hydrophobic region) in lipid bilayer has also been studied via MD simulations of a pure DPPC bilayer

Abbreviations: DPPC, dipalmitoylphosphatidylcholine; MD, molecular dynamics; DOPC, dioleoyl-phosphatidylcholine; VMD, Visual Molecular Dynamics; SPC, simple point charge; LINCS, linear constraint solver; PME, particle-mesh Ewald; PDF, probability density function; CDF, cumulative distribution function

* Correspondence to: G.H. Ding, Tel.: +86 21 50271866, fax: +86 21 50273866.
** Correspondence to: M. Karttunen, Tel.: +1 519 888 4567x31390.
E-mail addresses: 081029012@fudan.edu.cn1 (J.Y. Xie), ghding@fudan.edu.cn (G.H. Ding), mkarttu@gmail.com, mikko.karttunen@uwaterloo.ca (M. Karttunen).

0005-2736/$ – see front matter © 2014 Elsevier B.V. All rights reserved.
http://dx.doi.org/10.1016/j.bbamem.2013.12.011

[19]. The results demonstrated that the probability of stable pore formation depends on the number of water molecules in the hydrophobic region when no external force was applied. The presence of small nanoparticles in lipid bilayers was demonstrated to decrease the membrane rupture tension by enhancing the probability of water penetration [20]. Nevertheless, the previous systems focused mostly on the phenomenon of how external stimuli caused water pore formation or membrane rupture, and thus the lack of membrane dynamic properties in atomistic details caused the loss of critical quantitative description in the membrane rupture essence. To quantify the effects of membrane tension on lipid structure and dynamics, Muddana et al. performed MD simulations of DiI-labeled DPPC lipid bilayers under lateral tension [21]. The study provided insights into the relationship between tension and lipid dynamics, nevertheless, none information about membrane rupture has been described. In addition, coarse-grained simulations of pure DPPC bilayers under membrane tension have been conducted in both gel and liquid phases [22]. The latest simulations also shed light on the effect of membrane tension on the physical properties of pure DOPC lipid bilayers [23] but the tension was far from the lysis tension of a pure DOPC bilayer, which resulted in no pore formation observed in this study. To the best of our knowledge, dynamical properties of lipid bilayers under different lateral tensions or pressures, particularly during rupture, such as lipid area distribution, lipid ordering and tilting, have not yet been investigated in detail.

2. Material and methods

All MD simulations were performed with Gromacs v4.5.1 [24]. Visual Molecular Dynamics (VMD) [25] was used for all visualizations. For initial configurations, a DPPC lipid membrane from a previous 100 ns simulation was used[1] [26,27]. Two membrane sizes were used in the production simulations: A 128 DPPC system with 3655 water molecules and a larger bilayer of 512 DPPCs and 14620 water molecules which was constructed from the 128 DPPC systems. Force-field parameters for DPPC were taken from a previous developed lipid.itp file [28][2] and partial charges from the underlying model description [29]. For water, the simple point charge (SPC) model [30] was employed. All bonds were constrained to their equilibrium lengths with the linear constraint solver (LINCS) algorithm [31]. Periodic boundary conditions were applied. Lennard–Jones interactions and the real space part of electrostatic interactions were cut off at 1.0 nm. The particle-mesh Ewald (PME) method [32] was used to compute electrostatic interactions, since it has been shown that proper treatment of electrostatics is crucial in biomembrane systems [26,27,33,34]. For energy minimization, the steepest descent algorithm was used. All production MD simulations were done in the constant particle, pressure and temperature (NPT) ensemble with the V-rescale thermostat [35] at 323 K; the V-rescale thermostat has been shown to work very well in systems containing water and interfaces [33]. Surface tension was kept constant using the semi-isotropic Parrinello–Rahman pressure coupling algorithm [36,37] with the pressure set to 1 bar. The time step was set to 2.0 fs. Although the 128 DPPC systems were pre-equilibrated for 100 ns, both bilayers (128 and 512 lipids) were further equilibrated in the NPT ensemble for 100 ns. To ensure that equilibrium had been reached, we compared the area per lipid, order parameters, electrostatic potential, and the radial distribution functions to previous studies [26,27] and found full agreement.

To study the membranes' resistances to lateral tension and compression, we applied 1 bar, −50 bar, −100 bar, −200 bar, and 200 bar lateral pressure to the equilibrated 128 DPPC systems. A pressure of 1 bar was always applied in the normal direction. The corresponding surface tensions are 0 mN/m (1 bar), 17.93 mN/m (−50 bar), 30.79 mN/m (−100 bar), 44.78 mN/m (−200 bar), and −116.18 mN/m (200 bar). A pressure with positive value indicates compression while negative pressure means tension. In all former simulations, to our knowledge, tension was applied instantaneously [9,17,18,21–23]. We applied two different protocols: 1) high loading rate: −200 bar pressure was applied to the tension free membrane instantaneously and 2) low loading rate: −50 bar pressure was first applied for 10 ns. Then the pressure was changed to −100 bar for another 10 ns, and finally −200 bar pressure was applied. To gain insight into possible system size dependence, the same instantaneous lateral pressure of −200 bar was applied on both 128 DPPC and the larger 512 DPPC systems. Previous MD simulations have focused on the dependence of rupture at a specific lateral tension or lipid composition [9,17,18], or the lipid dynamic properties corresponding to several constant membrane tensions below rupture tension [21–23]. All production simulations lasted for 250 ns unless the membrane ruptured earlier. In all the figures, time 0 ns always corresponds to the beginning of the production simulation after which either the high or low loading protocol was applied.

The systems are labeled as follows: Normal Pressure (NP) for the pressure of 1 bar (reference system), T50 for −50 bar pressure, T100 for −100 bar pressure, LT200 for −200 bar pressure with low loading rate, HT200 for −200 bar pressure with high loading rate, BT200 for −200 bar pressure applied on 512 DPPC systems with high loading rate, and P200 for 200 bar pressure.

3. Results

3.1. Threshold of lateral tension for membrane rupture

The application of −200 bar lateral pressure always led to a rupture independent of the loading rate and membrane size. This is in agreement with previous simulations [9]. In the HT200 system, rupture occurred after about 6 ns, but it took about 35 ns for the BT200 system. The LT200 system remained intact for 50.2 ns after −200 bar pressure was reached, and after which it ruptured. In contrast, the T100 system remained stable for the full simulation time of 250 ns. Particularly, under lateral pressure loading of 200 bar, buckling of lipid bilayer was observed. The P200 system experienced a slight buckling deflection when lateral pressure was applied and remained stable through the whole simulation.

3.2. Membrane dimensions

One of the main bilayer characteristics is the average area per lipid molecule <A> (Fig. 1). As expected from 200 ns of pre-equilibration, the tensionless membrane was well equilibrated with $<A> = 0.656 \pm 0.010$ nm^2. This is in agreement with experiments and earlier MD studies [27,38,39]. As lateral tension increased, <A> increased noticeably. For T50, $<A> = 0.740 \pm 0.010$ nm^2, about 13% larger than the NP system, and for T100, $<A> = 0.867 \pm 0.010$ nm^2, about 32% increase. Finally, for LT200, $<A> = 1.178 \pm 0.020$ nm^2 before rupture, almost 80% larger than the reference system. For HT200, <A> remained at 1.199 ± 0.050 nm^2 only for 7 ns, followed by a rupture. In the BT200 system, $<A> = 1.226 \pm 0.050$ nm^2 for 45 ns followed by a rupture. Applying compression, P200, yielded $<A> = 0.441 \pm 0.001$ nm^2, which is 32.8% smaller than the reference value. The lipid membranes exposed to −200 bar lateral pressure had a transient state with area per lipid of ~1.2 nm^2 before rupture.

We also calculated the thickness of the bilayer defined as the average distance of P–P atoms in the lipid head groups (Fig. 2). For the NP system, we obtained 2.80 ± 0.05 nm. T50 gave 2.41 ± 0.05 nm, T100 1.97 ± 0.05 nm, LT200 before rupture 1.25 ± 0.05 nm, and P200 4.52 ± 0.05. When −200 bar pressure was applied, the thickness always remained at about 1.25 nm before rupture. HT200 stayed at 1.25 nm for only 3.5 ns, and then dropped to 1.0 nm abruptly within

[1] The topology file was available at http://www.softsimu.org/downloads/dppc-128-100.pdb.
[2] The force-field file was available at http://moose.bio.ucalgary.ca/files/lipid.itp.

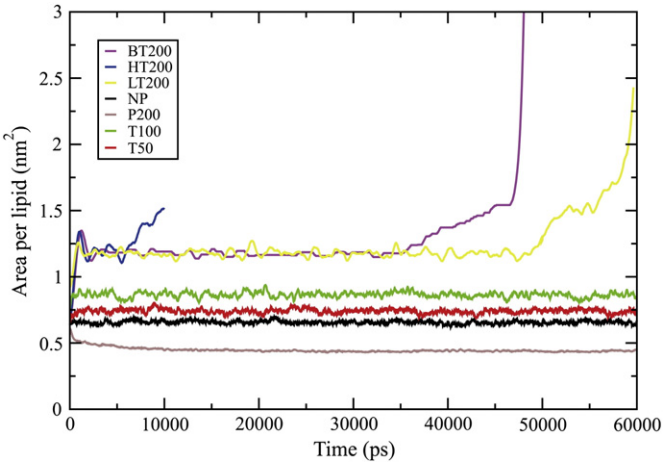

Fig. 1. Time evolution of the area per lipid. HT200, BT200, and LT200 rupture at different times while the other systems remained stable throughout the simulation (250 ns). 60 ns is shown for clarity. Time 0 ns corresponds to the beginning of the production simulation after which either the high or low loading protocol was applied.

2 ns. LT200 remained at 1.25 nm for almost 50 ns, and then fluctuated around 1.0 nm for another 10 ns. Similarly, BT200 stayed at 1.25 nm for 35 ns, and oscillated around 1.0 nm for the following 15 ns. This two-step behavior was observed independent of the loading rate and membrane size.

Area per lipid is an average property and does not contain information about the distribution of lipid molecules. To study possible changes in the lipids' distribution, we performed a Voronoi analysis in two dimensions to obtain the probability distributions for the area per lipid, P(A) [40]. Free areas, or voids, play a critical role in lipid membranes [41–43], and Voronoi analysis provides a method to describe them. In Voronoi tessellation, each lipid is first mapped onto the xy-plane. Next, the area that is closest to each of the lipids, called a Voronoi cell, is determined by a procedure similar to the Wigner–Seitz cell in solid state physics. We used the lipids' centers of masses for the mapping. The areas of the Voronoi cells give the area distribution (Fig. 3).

To obtain more precise descriptions of area distributions, all Voronoi samples were analyzed statistically (Table. 1) and fitted in terms of the probability density functions (PDF) [44]. To describe the distributions, the measured PDF is displayed as a histogram, while the theoretical PDF is displayed as a continuous curve fitted the histogram. We would like to point out that using a PDF is valid only for systems in equilibrium or steady-state.

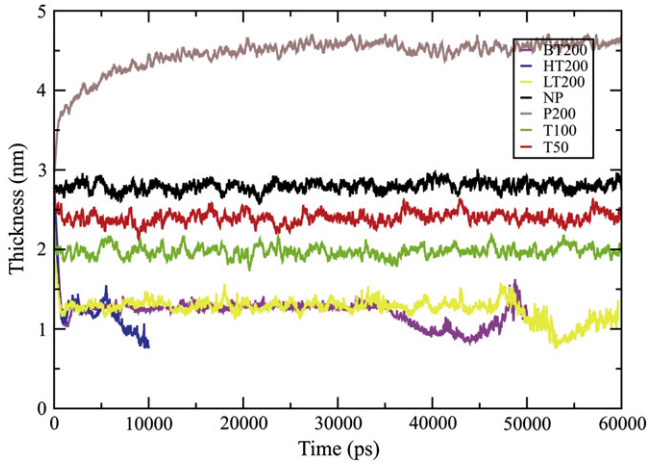

Fig. 2. Time evolution of membrane thickness. Calculated as the average distance of P–P atoms in the lipid head group. HT200, BT200, and LT200 rupture at different times. The other systems remained stable throughout the simulation (250 ns). 60 ns is shown for clarity.

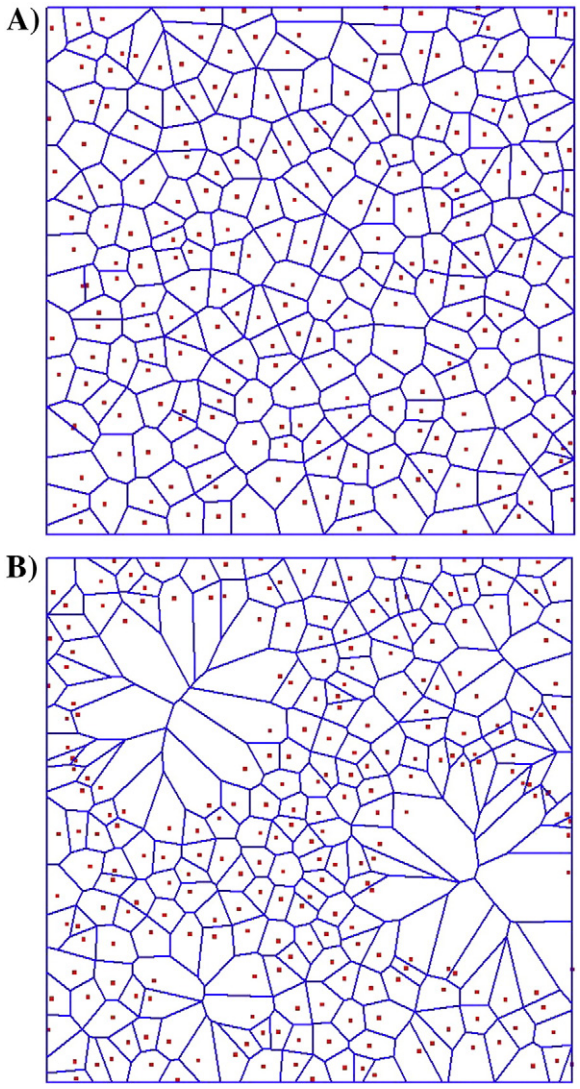

Fig. 3. Two dimensional Voronoi tessellation of the centers of mass of lipid molecules in the upper layer for (A) NP system and (B) BT200 system.

Due to the statistical uncertainty originating from relatively small systems (inherent limitation of MD) and hence limited amount of data, it is difficult to identify the unique distribution in each case. To avoid over-interpretation, instead of calculating the most precise function for each system, we compared the fittings to different distribution functions. The Kolmogorov–Smirnov [45] and Anderson–Darling tests [46] were used as statistical tests (Table. 2). The Kolmogorov–Smirnov statistic determines if a sample comes from a hypothesized continuous distribution, based on the largest vertical difference between the theoretical and the empirical cumulative distribution function. The Anderson–Darling procedure tests the fit of an observed cumulative distribution function to an expected one.

The results show that all the systems where membrane remains stable can be fitted in Dagum distribution [47] (Fig. 4). The Dagum distribution is often used in economics to characterize wealth distributions and it is also connected to the Gamma and Weibull distributions; the latter is often used in characterization of brittle fracture. In contrast, after the appearance of a water pore before rupture, the area distributions of LT200, HT200 and BT200 systems can no longer be fitted with a Dagum distribution but Burr distribution [48] seems to be a better

Table 1
Area distributions from Voronoi samples.

Area distribution								
Systems		Sample size	Mean	Variance	Standard deviation	Median	Skewness	Kurtosis
NP		1408	0.65864	0.029	0.17028	0.65085	0.45333	1.0972
T50		1408	0.73858	0.04083	0.20206	0.72885	0.42395	1.1516
T100		1408	0.8707	0.07085	0.26617	0.8467	0.60172	1.0063
P200		1408	0.44027	0.01244	0.11152	0.43455	0.28323	1.6473
HT200	Stable	1280	1.1196	0.17882	0.42288	1.0785	0.61051	1.42925
	With water pore	1280	1.3643	0.39509	0.62856	1.2325	1.7829	4.6571
LT200	Stable	1408	1.1803	0.14449	0.38011	1.138	0.84138	1.6573
	With water pore	1280	1.6727	1.1657	1.0797	1.3365	2.0818	5.4229
BT200	Stable	3072	1.1701	0.13565	0.3683	1.1375	0.60635	1.3905
	With water pore	2048	1.5057	1.1876	1.0898	1.2325	3.626	18.217

match (Fig. 4). The probability density function of three-parameter Dagum distribution is defined as:

$$f(x) = \frac{\alpha k \left(\frac{x}{\beta}\right)^{\alpha k - 1}}{\beta \left(1 + \left(\frac{x}{\beta}\right)^{\alpha}\right)^{k+1}}$$

where k is continuous shape parameter, α is the second continuous shape parameter, and β is continuous scale parameter (Table. 3). The probability density function of the three-parameter Burr Distribution (see the cautionary note above) is

$$f(x) = \frac{\alpha k \left(\frac{x}{\beta}\right)^{\alpha - 1}}{\beta \left(1 + \left(\frac{x}{\beta}\right)^{\alpha}\right)^{k+1}}$$

where k is continuous shape parameter, α is continuous shape parameter, and β is continuous scale parameter (Table. 3). We would like emphasize that fitting after water pore formation is somewhat questionable since the system is evolving and, strictly speaking, the distribution does not describe a well-defined steady-state but rather a transient.

To verify the goodness of fit, the cumulative distribution function (CDF), the probability difference graph that determines the difference between empirical CDF and theoretical CDF, the probability–probability (P–P) plot, and the quantile–quantile (Q–Q) plot are analyzed. To illustrate the goodness of the fit, the NP system is displayed as an example, and compared with Normal Distribution (Fig. 5).

All the plots are far from the Gaussian distribution [49]. To characterize the distribution data, skewness and kurtosis are calculated (Table. 1). Skewness is a measure of symmetry, and kurtosis is a measure of whether the data are peaked or flat relative to a normal distribution. Particularly, the skewness for a normal distribution is 0.0, and the kurtosis for a standard normal distribution is 3.0. The results of skewness and kurtosis confirm the above conclusion that none of the systems can be characterized by a Gaussian distribution.

Besides of the goodness of fit, which theoretically shows Dagum distribution and Burr distribution as best distributions, there are also physical reasons for the distribution selection. The Dagum distribution is a continuous probability distribution for non-negative real numbers. It is frequently encountered in the actuarial literature and mostly in the models on the size distribution of personal income [50–52]. Here, the Dagum distribution is able to describe the asymmetry of the area distribution.

The Burr distribution is a continuous probability distribution defined over all positive random variables, and is commonly used to model household income [52]. After the emergence of water pores, the size and position of membrane voids change rapidly, making the area distribution more and more scattered. Significant increase of skewness occurs during membrane rupture. Due to its flexible shape the Burr distribution is able to fit almost any given set of unimodal data [48,53]. Our fitting illustrates that the Burr distribution appears to provide a reasonable description of the area distribution after water pores start to form (caution: this is transient behavior and it is well possible the good fit to the Burr distribution simply describes a transient process).

To verify the consistency and correctness, the mean value of the Voronoi samples was determined (Table. 1) and found to be in agreement with the above average area per lipid. We examined the systems NP, T50, T100, and P200, where membrane always remained stable. The results illustrate that the variance as well as standard deviation is limited to small values (Table. 1). The membrane sustaining 200 bar lateral tension yields to slightly larger values during the temporary stable period, but gives rise to a significant increase after the water pore forms. The skewness value also indicates the formation of the water pore causing the distribution quite far from symmetry (Table. 1).

The parameters of Dagum distribution indicate that the shape of distribution is related to the applied force (Table. 3). In the compressed system, the distribution is concentrated with a larger α parameter,

Table 2
Kolmogorov–Smirnov, Anderson–Darling, and Chi-squared tests.

Area distribution function fitting test					
Systems		Distribution	Kolmogorov–Smirnov	Anderson–Darling	Chi-squared
NP		Dagum	0.0118	0.1326	6.3926
T50		Dagum	0.0124	0.1757	1.8779
T100		Dagum	0.0122	0.1599	2.5014
P200		Dagum	0.0286	1.3645	13.124
HT200	Stable	Dagum	0.0275	0.6747	14.114
	With water pore	Burr	0.0251	1.3474	10.122
LT200	Stable	Dagum	0.0125	0.2734	7.9463
	With water pore	Burr	0.0259	1.3033	13.795
BT200	Stable	Dagum	0.0158	1.5361	12.037
	With water pore	Burr	0.0237	1.6621	14.351

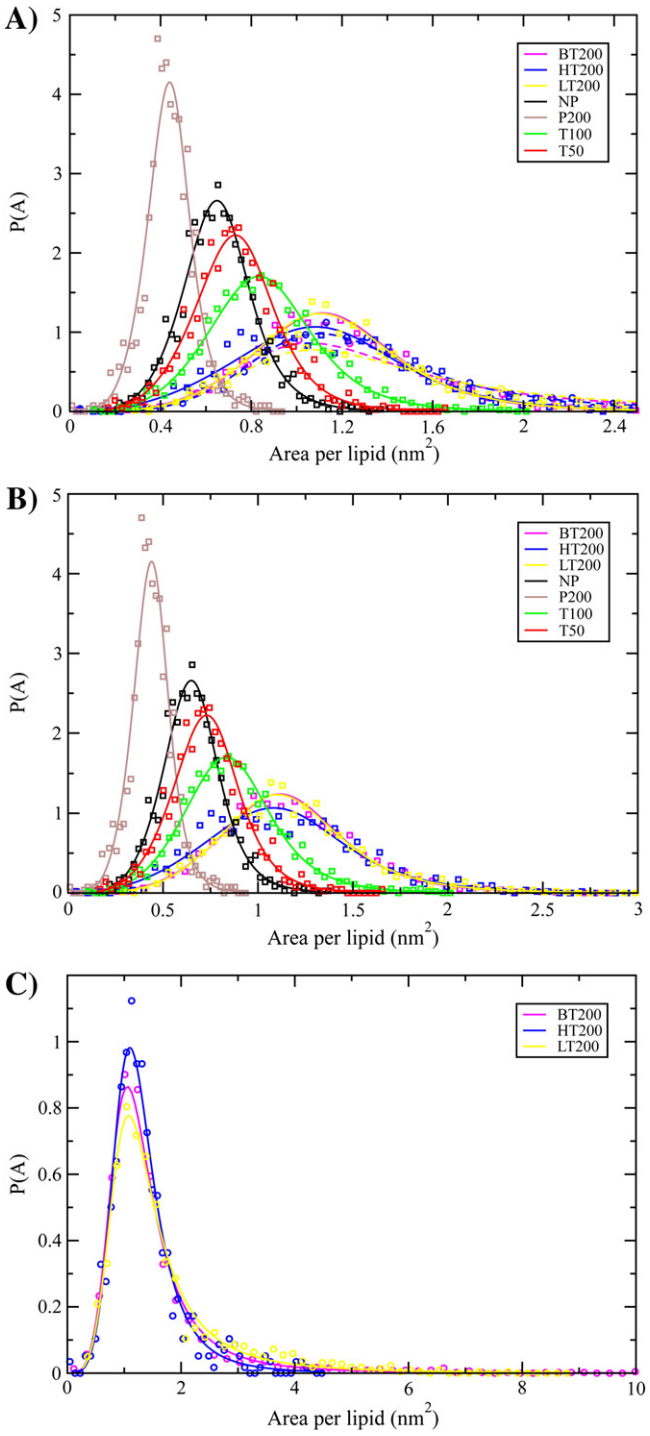

Fig. 4. (A) Probability density function of area distribution per lipid. The original data points are shown in discrete dots while the fits are shown in lines. The results of systems where water pore appears are shown in circles (data) or dotted lines (fit). (B) Same as (A) but only the systems where membrane remains stably are shown. All the area distributions are fitted to a Dagum distribution. (C) Same as (A) but only the systems where water pore appears are shown. All the area distributions are fitted to a Burr distribution.

while the larger tension causes a looser distribution according to the decreasing α parameters. Fig. 4 demonstrates 200 bar lateral tension: LT200 and BT200 have quite similar distribution shapes, whereas HT200 appears different: high loading rate leads to a sudden rupture suddenly without stabilizing process (redistribution). Once the water pore appears, the distribution ceases to follow a Dagum distribution.

Table 3
The fitting parameters of area distribution probability density function.

Area distribution function					
Systems		Distribution	Parameters		
			k	α	β
NP		Dagum	0.57329	8.6138	0.71947
T50		Dagum	0.53207	8.3907	0.82209
T100		Dagum	0.60449	7.0137	0.94955
P200		Dagum	0.52277	9.4691	0.48746
HT200	Stable	Dagum	0.52416	6.1446	1.3096
	With water pore	Burr	0.77142	4.9305	1.1449
LT200	Stable	Dagum	0.69132	6.3825	1.2448
	With water pore	Burr	0.49061	4.6738	1.0522
BT200	Stable	Dagum	0.63226	6.6965	1.2667
	With water pore	Burr	0.56723	4.7531	1.0296

This significant change between the stable and unstable states of the membrane is regarded as a signal of bilayer rupture.

3.3. Lipid ordering and tilt angle

The carbon–deuterium (CD) order parameter SCD is a measure for phospholipid chain ordering [54]. It is defined as:

$$S_{CD} = \frac{1}{2}\left(3\cos^2\theta - 1\right)$$

where θ is the angle between the membrane normal and the C – H bond vector. We computed SCD for both *sn-1* and *sn-2* chains (Fig. 6). When no lateral tension or pressure is applied on the membrane, the order parameter profile is found to be in good agreement with previous simulations [26] and experimental data [55–57]. When lateral tension is applied, the average order parameter drops from 0.160 in the NP system to 0.112 for T50, to 0.075 for T100, to 0.035 for LT200, and to 0.028 for HT200. The value for BT200, 0.038, is very close to the LT200. In the P200 system, the lipids become more ordered with average order parameter of 0.325.

Furthermore, the tilt of DPPCs, which was calculated as the angle between lipid chain and membrane normal vector and then averaged over all lipids, has been analyzed. The result demonstrates that the tilt angle depends strongly on the membrane lateral force. The larger tension gives rise to the more significant tilting, while in the P200 systems, lipids only have an average tilt angle of 15°, even less than the half value of tension free membrane. The analysis also illustrates that, during the transient stable period before rupture, the tilt angle is at around 49°. Since water pore forms, the tilt angle has a noticeable increase, and gives rise to a larger value of about 55°, till membrane fully ruptures.

To determine the effect of lateral force on the head group region of lipid bilayer, the angle between the phosphorus to nitrogen (P–N) vector and the membrane normal vector has been calculated. The result shows that the lipid head groups are oriented almost parallel to the bilayer surface due to the average angle being ~89.0°.

3.4. Lipid bilayer pressure profile

Lateral pressure profile is an important membrane property describing the local lateral (parallel to surface) pressure inside the membrane in the direction normal to the membrane surface [58–60]. For example, the interaction between water and hydrophobic hydrocarbon causes a significant local tension. Positive pressures arise predominantly from the chain conformational entropy and the head-group repulsions. To calculate the lateral pressure profile, the lipid bilayer is divided into ~0.1 nm thick slices, and the local pressure tensor in each slice is obtained by using the Irving–Kirkwood contour, which is described as a straight line connecting the particle pair [61,62]. The lateral pressure

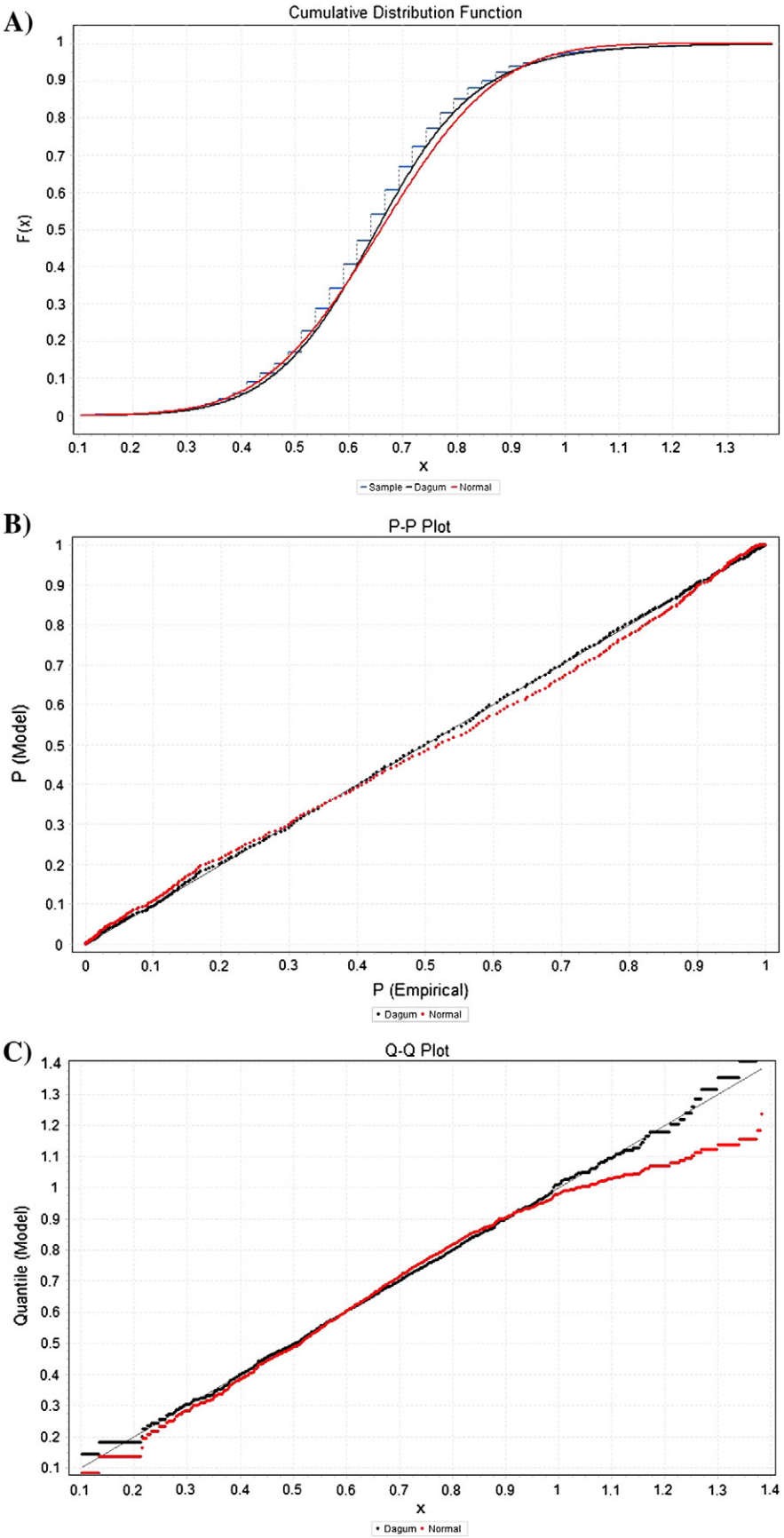

Fig. 5. (A) The cumulative distribution function (CDF), (B) the probability–probability (P–P) plot, (C) the quantile–quantile (Q–Q) plot, and (D) the probability difference plot of Dagum distribution in NP system, compared with Gaussian distribution.

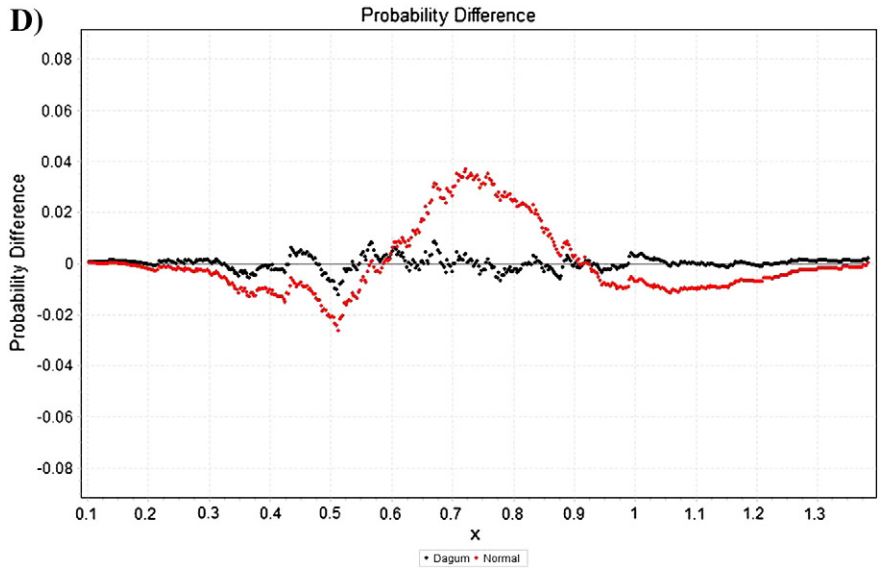

Fig. 5 (*continued*).

profile π(z) is the difference between the normal and the lateral pressure tensor [63–65]:

$$\pi(z) = \left(P_{xx} + P_{yy}\right)/2 - P_{zz}.$$

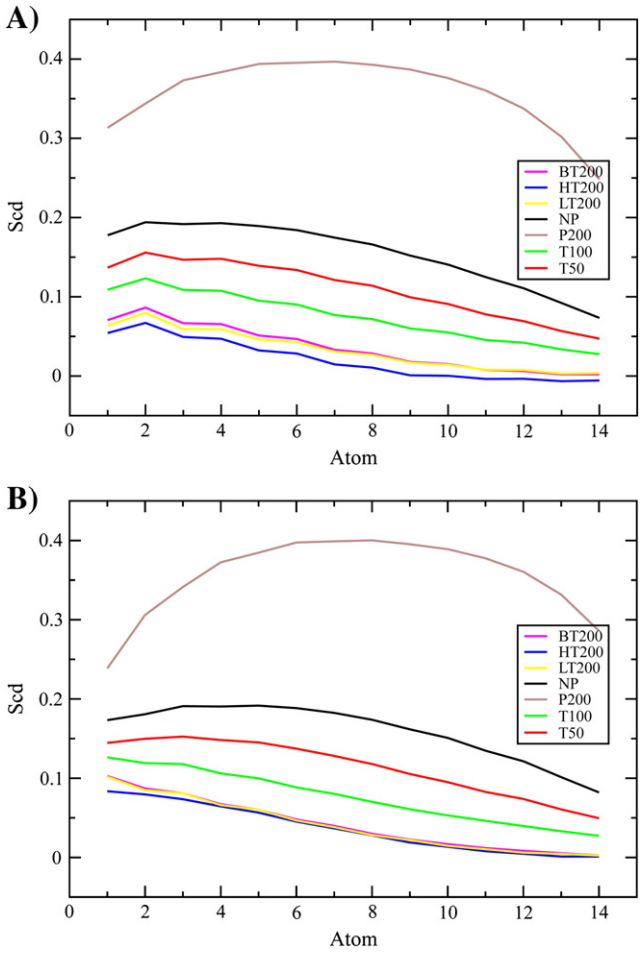

Fig. 6. Order parameter SCD for both *sn-1* (A) and *sn-2* (B).

Positive lateral pressure profile indicates that the bilayer tends to expand along the lateral direction, while negative values imply contraction. In our simulations, the lateral pressure profile of pure DPPC bilayer at zero tension is in good agreement with earlier MD simulations [66–68]. The lateral pressure profiles (Fig. 7) indicate that from NP to T50 and then to T100, the negative peak at the boundary between the water and hydrophobic hydrocarbon regions increases noticeably. In the P200 system, the negative peak decreases and the positive peak at the head-group region increases at the same time. It is notable that although the absolute values of the peaks are strongly influenced by the applied pressure, the qualitative features remain the same. If embedded proteins would be present, their function would be influenced by large quantitative changes [60]. The profiles have been smoothed by cubic spline fitting and averaged over the two leaflets.

3.5. Membrane rupture

To determine how rupture depends on lateral tension and loading rate, different loading rates were applied. In the HT200 system, spontaneous rupture occurred after 6 ns. This is consistent with former MD simulations of DPPC membranes [9,18]. When a slow loading rate (LT200) was applied, it took 50 ns from the time when −200 bar was applied, more than 8 times longer compared to the HT200 system, for the membrane to rupture. For the BT200 system, rupture started at

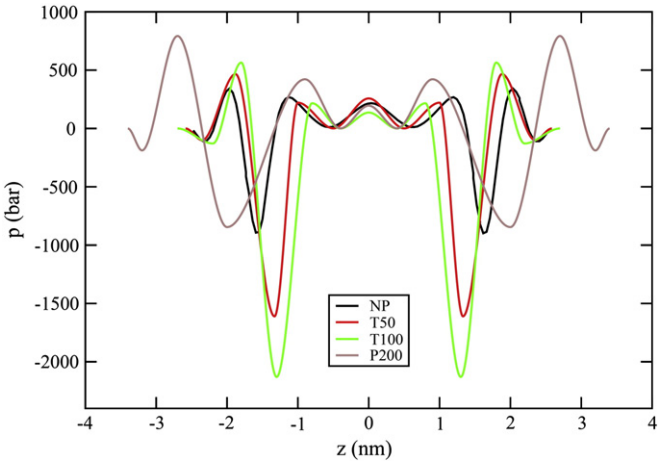

Fig. 7. Lateral pressure profiles through the lipid bilayer.

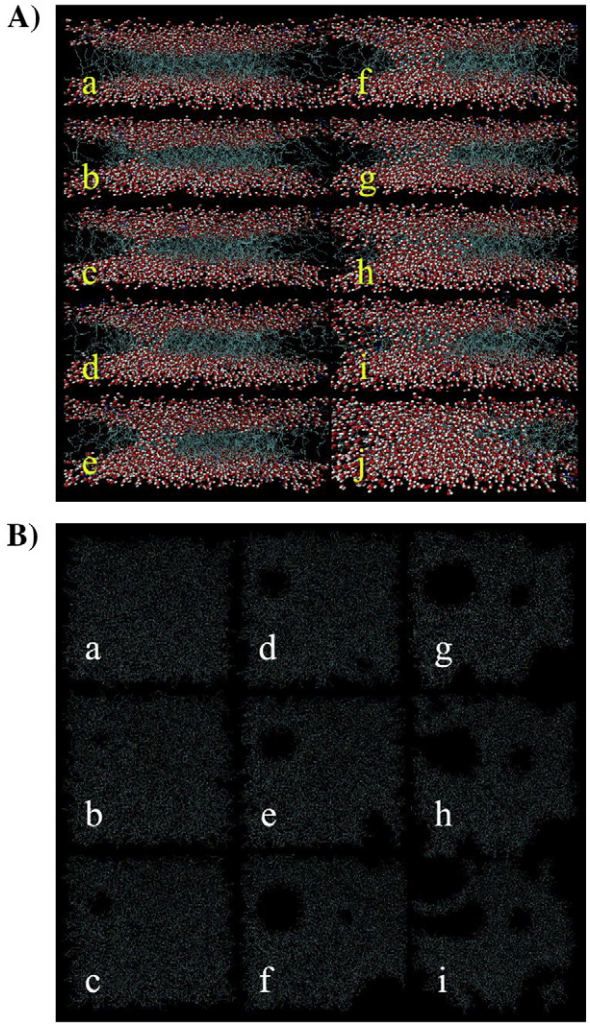

Fig. 8. Water pore formation during simulation with lateral pressure of −200 bar. (A) The plots are shown in the side direction, where lipids are shown in green chains and water in white and red points. (B) The plots are shown from the top, where only lipids are shown.

35 ns after −200 bar was applied. The results suggest that the tension at which rupture occurs depends strongly on the rate at which it is applied. This is in agreement with pipette aspiration studies [14–16]. With smaller tensions (T50 and T100), no rupture was observed even in time scales of 250 ns. Additionally, membrane rupture has a strong relationship with the model size. Sustaining to the same lateral tensions, membrane with larger size gives rise to a longer stable time before water pore forms.

The results also imply that the rupture of a lipid is a spontaneous incident rather than a slow changing process. When −200 bar pressure was applied on the system directly (HT200), at the beginning all the data were found too close to the values in the stable system with −200 bar pressure applying in slow loading rate (LT200), but the measurements changed suddenly and significantly after lipids rupture. It took only 4 ns from the beginning of water pore forms to the membrane fully break down.

Carefully examining the conformations, once the lateral pressure reaches the critical value of −200 bar, the lipid molecules start to rearrange significantly and the fluctuations induced in the lipid matrix result in the formation of a water pore. The pores are stabilized at low loading rate. In contrast, under high loading rate, water pores expand and the membrane becomes unstable. The pore formation starts with the penetration of water molecules from both sides of the membrane, and continues to increase the radius. When the water molecules meet in the middle of the bilayer, a complete water channel is created, adopting an hourglass shape. Once one water channel is formed, a gradual expansion of the channel is observed and several new channels emerge quickly, leading to membrane rupture (Fig. 8). Different MD simulations of hydrophilic pores in lipid bilayers confirm our result and demonstrate that irreversible membrane breakdown occurs once the expansion of the pore (water channel) reaches a threshold radius [9,17,18]. These previous studies were inclined to focus on the formation of a single pore. However, in our simulations, the number of water pores is proportional to the membrane size. In the HT200 system, one pore was enough to rupture the membrane, while in the BT200 system, the formation of the first pore triggered other water pores before rupture. The lipid head-groups within the pore rearrange during the expansion, while their relative population is constant, and the thickness of the bilayer remains the same. Only when the rupture occurs is the gradual thinning of the bilayer concomitant with the overturn of lipid molecules.

4. Discussion and conclusions

The behavior of DPPC lipid membranes corresponding to different lateral forces was investigated by MD simulations. Our simulations show that the loading rate has an impact on membrane behavior. Membranes appear more resistant at slower loading rate, which confirms the micropipette aspiration experiments [14–16]. When an external force is applied gradually, the lipid bilayer has time to react and rearrange the lipids. Instantaneously application of an external force easily leads to a rapid rupture. Rupture is characterized by the appearance of unstable growing water pores. The stability of the pores depends on the rate at which loading is applied. Experiments show that at low loading rates, the kinetics of rupture depend on the rate at which the pore can expand, while at high loading rates, the formation of the pore itself becomes rate-limiting [14,15]. Thus, at high loading rates the tension required for pore formation is relatively high, inevitably leading to membrane rupture. We also tested the size dependence of the rupture process. Our results demonstrate that larger membranes show more resistance to lateral tension and are able to remain intact for a longer time before final rupture.

In our simulations, rupture occurred under a membrane pressure of −200 bar independent of the loading rate and membrane size. Rupture occurred through the formation of water pores accompanied by the transformation of area probability distribution from a Dagum distribution to Burr Distribution. Other properties, such as the area per lipid, ordering and tilting of lipid molecules, allowed us to quantify the behavior of the lipid membrane during rupture at the atomic level, and provide a reference for future experiments.

Acknowledgements

We thank the Natural Sciences and Engineering Research Council (NSERC) of Canada (MK), the National Basic Research Program of China (2012CB518502), and the China Scholarship Council (CSC) (no. 2011610047) for financial support. SharcNet [www.sharcnet.ca] is acknowledged for computational resources.

References

[1] H.D. Huang, R.D. Kamm, R.T. Lee, Cell mechanics and mechanotransduction: pathways, probes, and physiology, Am. J. Physiol. 287 (2004) C1–C11.
[2] K.L. Marshall, E.A. Lumpkin, The molecular basis of mechanosensory transduction, Adv. Exp. Med. Biol. 739 (2012) 142–155.
[3] E.S. Haswell, R. Phillips, D.C. Rees, Mechanosensitive channels: what can they do and how do they do it? Structure 19 (10) (Oct 12 2011) 1356–1369.
[4] K. Olbrich, W. Rawicz, D. Needham, E. Evans, Water permeability and mechanical strength of polyunsaturated lipid bilayers, Biophys. J. 79 (2000) 321–327.
[5] W. Rawicz, B.A. Smith, T.J. McIntosh, S.A. Simon, E. Evans, Elasticity, strength, and water permeability of bilayers that contain raft microdomain-forming lipids, Biophys. J. 94 (2008) 4725–4736.
[6] P.J. Butler, T.C. Tsou, J.Y.S. Li, S. Usami, S. Chien, Rate sensitivity of shear-induced changes in the lateral diffusion of endothelial cell membrane lipids: a role for

membrane perturbation in shear-induced MAPK activation, FASEB J. 15 (2001) 216–218.
[7] P.J. Butler, G. Norwich, S. Weinbaum, S. Chien, Shear stress induces a time- and position-dependent increase in endothelial cell membrane fluidity, Am. J. Physiol. 280 (2001) C962–C969.
[8] A.J. Garcia-Saez, S. Chiantia, P. Schwille, Effect of line tension on the lateral organization of lipid membranes, J. Biol. Chem. 282 (2007) 33537–33544.
[9] P.D. Tieleman, H. Leontiadou, A.E. Mark, S.J. Marrink, Simulation of pore formation in lipid bilayers by mechanical stress and electric fields, J. Am. Chem. Soc. 2003 (125) (2003) 6382–6383.
[10] J. Akinlaja, F. Sachs, The breakdown of cell membranes by electrical and mechanical stress, Biophys. J. 75 (1998) 247–254.
[11] M.A. Haidekker, N.L. Heureux, J.A. Frangos, Fluid shear stress increases membrane fluidity in endothelial cells: a study with DCVJ fluorescence, Am. J. Physiol. Heart Circ. Physiol. 278 (2000) H1401–H1406.
[12] J.S. Oghalai, H.B. Zhao, J.W. Kutz, W.E. Brownell, Voltage- and tension-dependent lipid mobility in the outer hair cell plasma membrane, Science 287 (2000) 658–661.
[13] J.B. de Monvel, W.E. Brownell, M. Ulfendahl, Lateral diffusion anisotropy and membrane lipid/skeleton interaction in outer hair cells, Biophys. J. 91 (2006) 364–381.
[14] E. Evans, V. Heinrich, F. Ludwig, W. Rawicz, Dynamic tension spectroscopy and strength of biomembranes, Biophys. J. 85 (2003) 2342–2350.
[15] E. Evans, V. Heinrich, Dynamic strength of fluid membranes, C.R. Phys. 4 (2003) 265–274.
[16] A. Ikai, R. Afrin, Toward mechanical manipulations of cell membranes and membrane proteins using an atomic force microscope: an invited review, Cell Biochem. Biophys. 39 (2003) 257–277.
[17] R.D. Groot, K.L. Rabone, Mesoscopic simulation of cell membrane damage, morphology change and rupture by nonionic surfactants, Biophys. J. 81 (2001) 725–736.
[18] H. Leontiadou, A.E. Mark, S.J. Marrink, Molecular dynamics simulations of hydrophilic pores in lipid bilayers, Biophys. J. 86 (2004) 2156–2164.
[19] K. Koshiyama, T. Yano, T. Kodama, Self-organization of a stable pore structure in a phospholipid bilayer, Phys. Rev. Lett. 105 (2010) 018105.
[20] K. Lai, B. Wang, Y. Zhang, Y. Zheng, Computer simulation study of nanoparticle interaction with a lipid membrane under mechanical stress, Phys. Chem. Chem. Phys. (2012) 19.
[21] H.S. Muddana, R.R. Gullapalli, E. Manias, P.J. Butler, Atomistic simulation of lipid and DiI dynamics in membrane bilayers under tension, Phys. Chem. Chem. Phys. 13 (2011) 1368–1378.
[22] J. Neder, B. West, P. Nielaba, F. Schmid, Coarse-grained simulations of membranes under tension, J. Chem. Phys. 132 (2010) 115101.
[23] A. Srinivas Reddy, D.T. Warshaviak, M. Chachisvilis, Effect of membrane tension on the physical properties of DOPC lipid bilayer membrane, Biochim. Biophys. Acta 1818 (2012) 2271–2281.
[24] B. Hess, C. Kutzner, D.V. Spoel, E. Lindahl, GROMACS 4: algorithms for highly efficient, load-balanced, and scalable molecular simulation, J. Chem. Theory Comput. 4 (2008) 435–447.
[25] W. Humphrey, A. Dalke, K. Schulten, VMD — Visual Molecular Dynamics, J. Mol. Graphics 14 (1996) 33–38.
[26] M. Patra, M. Karttunen, M. Hyvonen, E. Falck, P. Lindqvist, I. Vattulainen, Molecular dynamics simulations of lipid bilayers: major artifacts due to truncating electrostatic interactions, Biophys. J. 84 (2003) 3636–3645.
[27] M. Patra, M. Karttunen, M. Hyvonen, E. Falck, I. Vattulainen, Lipid bilayers driven to a wrong lane in molecular dynamics simulations by subtle changes in long-range electrostatic interactions, J. Phys. Chem. B 108 (2004) 4485–4494.
[28] O. Berger, O. Edholm, F. Jahnig, Molecular dynamics simulations of a fluid bilayer of dipalmitoylphosphatidylcholine at full hydration, constant pressure, and constant temperature, Biophys. J. 72 (1997) 2002–2013.
[29] D.P. Tieleman, H.J.C. Berendsen, Molecular dynamics simulations of a fully hydrated dipalmitoylphosphatidylcholine bilayer with different macroscopic boundary conditions and parameters, J. Chem. Phys. 105 (1996) 4871–4880.
[30] H.J.C. Berendsen, J.P.M. Postma, W.F. van Gunsteren, J. Hermans, Interaction models for water in relation to protein hydration, in: B. Pullman (Ed.), Intermolecular Forces, Reidel, Dordrecht, The Netherlands, 1981, pp. 331–342.
[31] B. Hess, H. Bekker, H.J.C. Berendsen, J.G.E.M. Fraaije, LINCS: a linear constraint solver for molecular simulations, J. Comput. Chem. 18 (1997) 1463–1472.
[32] U. Essman, L. Perera, M.L. Berkowitz, H.L.T. Darden, L.G. Pedersene, A smooth particle mesh Ewald method, J. Chem. Phys. 103 (1995) 8577–8592.
[33] J. Wong-ekkabut, M. Miettinen, C. Dias, M. Karttunen, Static charges cannot drive a continuous flow of water molecules through a carbon nanotube, Nat. Nanotechnol. 5 (2010) 555–557.
[34] M. Karttunen, J. Rottler, I. Vattulainen, C. Sagui, Electrostatics in biomolecular simulations: where are we now and where are we heading, Curr. Top. Membr. 60 (2008) 49–89.
[35] G. Bussi, D. Donadio, M. Parrinello, Canonical sampling through velocity rescaling, J. Chem. Phys. 126 (2007) 014101.
[36] S. Nose, M. Klein, Constant pressure molecular dynamics for molecular systems, Mol. Phys. 50 (1983) 1055–1076.
[37] M. Parrinello, A. Rahman, Polymorphic transitions in single crystals: a new molecular dynamics method, J. Appl. Phys. 52 (1981) 7182–7190.
[38] J.F. Nagle, S. Tristram-Nagle, Structure of lipid bilayers, Biochim. Biophys. Acta 1469 (2000) 159–195.
[39] S. Leekumjorn, A.K. Sum, Molecular simulation study of structural and dynamic properties of mixed DPPC/DPPE bilayers, Biophys. J. 90 (2006) 3951–3965.
[40] W. Shinoda, S. Okazaki, A Voronoi analysis of lipid area fluctuation in a bilayer, J. Chem. Phys. 109 (1998) 1517–1521.
[41] M. Kupiainen, E. Falck, S. Ollila, P. Niemelä, A.A. Gurtovenko, M.T. Hyvönen, M. Patra, M. Karttunen, I. Vattulainen, Free volume properties of sphingomyelin, DMPC, DPPC, and PLPC bilayers, J. Comput. Theor. Nanosci. 2 (2005) 401–413.
[42] E. Falck, M. Patra, M. Karttunen, M.T. Hyvönen, I. Vattulainen, Impact of cholesterol on voids in phospholipid membranes, J. Chem. Phys. 121 (2004) 12676.
[43] E. Falck, M. Patra, M. Karttunen, M.T. Hyvönen, I. Vattulainen, Lessons of slicing membranes: interplay of packing, free area, and lateral diffusion in phospholipid/cholesterol bilayers, Biophys. J. 87 (2004) 1076–1091.
[44] N.G. Ushakov, Density of a probability distribution, in: Michiel Hazewinkel (Ed.), Encyclopedia of Mathematics, Springer, 2001, (ISBN 978-1-55608-010-4).
[45] A.N. Kolmogorov, Sulla determinazione empirica di una legge di distribuzione, G. Inst. Ital. Attuari. 4 (1933) 83.
[46] M.A. Stephens, EDF statistics for goodness of fit and some comparisons, J. Am. Stat. Assoc. 69 (1974) 730–737.
[47] Christian Kleiber, A guide to the Dagum distributions, in: Duangkamon Chotikapanich (Ed.), Modeling Income Distributions and Lorenz Curves (Economic Studies in Inequality, Social Exclusion and Well-being), Springer, 2008, (Chapter 6).
[48] I.W. Burr, Cumulative frequency functions, Ann. Math. Stat. 13 (1942) 215–232.
[49] George Casella, Roger L. Berger, Statistical Inference, 2nd ed. Duxbury, 2001. (ISBN 0-534-24312-6).
[50] Camilo Dagum, A model of income distribution and the conditions of existence of moments of finite order, Proceeding of the 40th Session of the ISI, Contributed Paper, Bulletin of the International Statistical Institute, 46, 1975, pp. 199–205.
[51] Camilo Dagum, A new model of personal income distribution: specification and estimation, Econ. Appl. 30 (1977) 413–437.
[52] Christian Kleiber, Samuel Kotz, Statistical Size Distributions in Economics and Actuarial Sciences, Wiley, Hoboken, NJ, 2003, ISBN 0-471-15064-9.
[53] Pandu R. Tadikamalla, A look at the burr and related distributions, Int. Stat. Rev. 48 (1980) 337–344.
[54] D.P. Tieleman, S.J. Marrink, H.J.C. Berendsen, A computer perspective of membranes: molecular dynamics studies of lipid bilayer systems, Biochim. Biophys. Acta Biomembr. 1331 (1997) 235–270.
[55] M.F. Brown, J. Seelig, U. Haberlen, Structural dynamics in phospholipid bilayers from deuterium spin–lattice relaxation time measurements, J. Chem. Phys. 70 (1979) 5045–5053.
[56] J.P. Douliez, A. Leonard, E.J. Dufourc, Restatement of order parameters in biomembranes: calculation of C– C bond order parameters from C–D quadrupolar splittings, Biophys. J. 68 (1995) 1727–1739.
[57] H.I. Petrache, S.W. Dodd, M.F. Brown, Area per lipid and acyl length distributions in fluid phosphatidylcholines determined by ^{2}H NMR spectroscopy, Biophys. J. 79 (2000) 3172–3192.
[58] Samuli Ollila, Lateral Pressure in Lipid Membranes and Its Role in Function of Membrane, Proteins, http://URN.fi/URN:NBN:fi:tty-201011181369.
[59] P.S. Niemela, S. Ollila, M.T. Hyvonen, M. Karttunen, I. Vattulainen, Assessing the nature of lipid raft membranes, PLoS Comput. Biol. 3 (2007) e34.
[60] S. Ollila, T. Róg, M. Karttunen, I. Vattulainen, Role of sterol type on lateral pressure profiles of lipid membranes affecting membrane protein functionality: comparison between cholesterol, desmosterol, 7-dehydrocholesterol and ketosterol, J. Struct. Biol. 159 (2007) 311–323.
[61] J.G. Kirkwood, F.P.J. Buff, The statistical mechanical theory of surface tension, J. Chem. Phys. 17 (1949) 338–343.
[62] J.H. Irving, J.G. Kirkwood, The statistical mechanical theory of transport processes. IV. The equations of hydrodynamics, J. Chem. Phys. 18 (1950) 817–829.
[63] J.S. Rowlinson, B. Widom, Molecular Theory of Capillarity, Clarendon Press, Oxford, 1982.
[64] S.A. Safran, Statistical Thermodynamics of Surfaces, Interfaces, and Membranes, Addison-Wesley, Reading, MA, 1994.
[65] D. Marsh, Lateral pressure in membranes, Biochim. Biophys. Acta 1286 (1996) 183–223.
[66] E. Lindahl, O. Edholm, Spatial and energetic–entropic decomposition of surface tension in lipid bilayers from molecular dynamics simulations, J. Chem. Phys. 113 (2000) 3882–3893.
[67] J. Sonne, F.Y. Hansen, G.H. Peters, Methodological problems in pressure profile calculations for lipid bilayers, J. Chem. Phys. 122 (2005) 124903.
[68] M. Patra, Lateral pressure profiles in cholesterol-DPPC bilayers, Eur. Biophys. J. 35 (2005) 79–88.